Materials and Design 182 (2019) 107972

Contents lists available at ScienceDirect

Materials and Design

journal homepage: www.elsevier.com/locate/matdes

Vanadium oxide anchored MWCNTs nanostructure for superior symmetric electrochemical supercapacitors

Shilpa A. Pande [a,*], Bidhan Pandit [b,*], Babasaheb R. Sankapal [b]

[a] Dept of Applied Physics, Laxminarayan Institute of Technology, R T M Nagpur University, Nagpur 440033, Maharashtra, India
[b] Nano Materials and Device Laboratory, Department of Physics, Visvesvaraya National Institute of Technology, South Ambazari Road, Nagpur 440010, Maharashtra, India

HIGHLIGHTS

- Complete symmetric supercapacitor device with a wide voltage frame of 2 V.
- Highest recordable specific capacitance of 569.7 F/g at 2 mV/s scan rate.
- Remarkable energy density of 62 Wh/kg and power density of 11.5 kW/kg with capacitive retention of 89.2 % for 4000 cycles.
- Glowing of red LED shows the practical aspect of device.

GRAPHICAL ABSTRACT

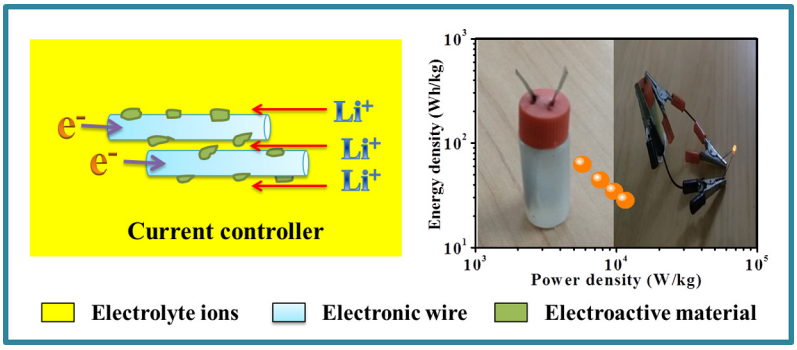

ARTICLE INFO

Article history:
Received 8 April 2019
Received in revised form 22 June 2019
Accepted 24 June 2019
Available online 25 June 2019

Keywords:
Nanocomposite
Energy storage
Symmetric supercapacitor
Wide voltage window

ABSTRACT

Proper selection of electrode material with sensible scheme is definitely significant to dodge commercial obstacles of supercapacitors. This challenge has been addressed by engineering prototype symmetric supercapacitor (SSC) device fabricated with enhanced supercapacitive vanadium (V) oxide integrated multi-walled carbon nanotubes (MWCNTs) composite as electrode material with Li-ion associating $LiClO_4$ electrolyte. The V_2O_5/MWCNTs composite with nanoscale architecture has been synthesized with inexpensive and simple chemical bath deposition (CBD) method. The cyclic voltammetry of SSC device has exhibited the involvement of electrochemically active reversible redox process in the composite. The specific capacitance of 569.7 F/g at scan rate of 2 mV/s including excellent electrochemical stability of 89.2% at 4000 CV cycles have been achieved with operating potential window of 2 V. Furthermore, the device exhibits excellent energy density of 62 Wh/kg and exceptional power density of 11.5 kW/kg. The low resistive factors have driven the device towards the potential application as glowing of red LED for 10 s.

1. Introduction

Due to energy snags, unfathomable efforts have been made to design novel supercapacitors (SCs), which have been measured as potential energy storage solutions due to their necessary assets of pronounced power density (ten times greater than orthodox batteries), quick charge/discharge, exceptional lifetime, light weight and compact size

* Corresponding authors.
E-mail addresses: sap7001@gmail.com (S.A. Pande), physics.bidhan@gmail.com (B. Pandit).

https://doi.org/10.1016/j.matdes.2019.107972

[1]. However, there are several obstacles in developing high performance SCs due to restrictions regarding to both the electrolyte and electrode components. The performance of supercapacitors is not only dependent on the electrode materials, but also strongly affected by the employed electrolytes [2]. The environmental points and favorable cost of SCs associating with aqueous electrolytes are influential; still, advancement towards inexpensive and high specific capacitance SCs poses a substantial challenge.

Electrochemical capacitors centred on transition metal oxides showed remarkable capacitance with better electrochemical stability than the conventional conducting polymers and carbon materials [3]. Previously, ruthenium oxide was one of the most promising metal oxide electrodes for electrochemical supercapacitor owing to its extraordinary specific capacitance. However, the cost of this novel metal oxide is too expensive to commercialize, efforts have being made towards exploration on alternative electrode materials for supercapacitor to achieve better electrochemical properties.

The thin layer of V_2O_5 is being considered the topic of research in current years due to their structure, morphology, physical and corresponding chemical characteristics, which lead towards various real-world applications. V_2O_5 is specified by layered structure in which the alkaline atoms can reversibly deintercalated after being intercalated [4]. As a result, V_2O_5 as intercalation compound has attracted a lot for electrochemical pseudocapacitor application. In precise case, single V_2O_5 unit can take part in insertion/extraction up to three lithium ions, resulting a total capacity of 440 mAh/g in voltage frame of 1.5–3.8 V [5]. On the other hand, combining V_2O_5 with conductive carbon nanomaterials has been justified to be an efficient method to improve not only the electric transport properties, but the cyclic stability by enhancing adhesion with nanostructures [6–8]. Wu et al. prepared V_2O_5/MWCNTs hybrid which exhibit outstanding capacitance of 625 F/g with excellent cyclic stability (> 20,000 cycles) [9]. With the help of hydrothermal process, Lee et al. synthesized graphene decorated V_2O_5 with enhanced specific capacitance of 288 F/g [10]. Furthermore, the V_2O_5/carbon nanofiber composite exhibits improved capacitance of 150 F/g with higher energy density of 18.8 Wh/kg as reported by Kim et al. [11].

As various application requires minimum operating voltage of 1.5 V, many efforts have been put forth to widen the potential window of supercapacitor above 1.5 V for single device by combining asymmetric or symmetric device configurations. Asymmetric configuration involved two dissimilar electrode materials whereas symmetric involves both electrodes of same material. Designing and making it industry scalable, symmetric configuration is easy and cost effective. It requires two electrodes coated with active material and sandwiched by using membrane/separator which is soaked with liquid electrolyte for liquid configured device. Hence, efforts have been put forth to assemble symmetric configured supercapacitive device with widen potential window of 2.0 V.

An attempt has been made to synthesize V_2O_5 by simple and inexpensive chemical bath deposition (CBD) method to design the supercapacitor device in aqueous electrolyte. Present study emphasizes (i) exploitation of easy CBD method to prepare V_2O_5 nanostructure onto 'dip and dry' coated stable and conductive MWCNTs nanonetwork, (ii) symmetric supercapacitor (SSC) device fabrication using nanoscale V_2O_5 architecture with improved electro-active cavities for $LiClO_4$ electrolyte to penetrate, and (iii) improved capacitance and power/energy density values with decent cyclic stability in well-defined steady manner.

2. Experimental techniques

2.1. Synthesis of V_2O_5/MWCNTs thin film

The MWCNTs film on stainless steel (SS) substrate was prepared by easy 'dip and dry' process as illustrated in our previous report [12]. Now, V_2O_5 was synthesized by adopting simple CBD method. Ionic and solubility product plays a vibrant role for CBD method. Normally the ionic product of both anion and cation will comparable with the solubility product of consisting oxide in saturation condition for CBD method. While it exceeds, ions combine and precipitation follows on substrate as form of deposition. First, 0.4 ml of 1 M NaOH was added drop wise in aqueous $VOSO_4$ solution (0.1 M) to obtain a blue colored uniform solution by preparing vanadyl ion (VO^{2+}) bath. The homogeneous solution was maintained at 60 °C for 3 h with continuous stirring of 100 rpm to get green colored V_2O_5 nanostructure on MWCNTs substrate which was dipped initially in the solution. At the MWCNTs surface, the ionic cluster of VO_2^+ is oxidized to deposit solid V_2O_5 through the providing reaction [13]:

$$2VO^{2+} + 3H_2O \overset{60\,^{\circ}C}{\rightarrow} V_2O_5 + 6H^+ + 2e^- \quad (1)$$

Briefly, the process consists of two states. Primarily VO^{2+} oxidizes to soluble $H_2V_{10}O_{28}^{4-}$:

$$10VO^{2+} + 18H_2O \rightarrow H_2V_{10}O_{28}^{4-} + 34H^+ + 10e^- \quad (2)$$

And in next stage precipitation occurs in the electrode interface:

$$H_2V_{10}O_{28}^{4-} + 4H^+ \rightarrow 5V_2O_5 + 3H_2O \quad (3)$$

The precipitation initially dispersed in the solution and consequently condensed on the MWCNTs substrate. To achieve uniform deposition of V_2O_5 on MWCNTs substrate, the solution was stirred at speed of 100 rpm throughout the procedure. Finally, the substrate was dried at room temperature (28 °C) after being rinsed with double distilled water (DDW).

The mass loading of V_2O_5/MWCNT film on SS substrate is 0.26 mg/cm^2. So, the total mass loading involved in (1×1) cm^2 prototype device is $(m_1 + m_2) = (0.26 + 0.26)$ mg $= 0.52$ mg. Here, m_1 and m_2 are the masses of positive and negative electrodes. As the reported cell is a symmetric device, then $m_1 = m_2 = 0.26$ mg.

The structural, morphological and electrochemical characterization techniques have been briefly discussed in Supplementary information S1.

3. Results and discussion

3.1. Structural studies

The crystal structure formation of V_2O_5 thin film on SS substrate was collected by X-ray diffraction (XRD) as depicted in Fig. 1a. XRD analysis of V_2O_5 thin film clearly indicates a prominent peak at $2\theta = 25.5°$ which resembles to the (210) crystal plane of V_2O_5 (JCPDS No. 89–2483) with orthorhombic structure. A small peak at $2\theta = 25.8°$ associates with (002) crystal plane of MWCNTs whereas the extra peaks (denoted by 'Δ') are for SS substrate [14].

An FTIR spectrum (Supplementary information S2) of as synthesized orthorhombic V_2O_5 sample was recorded to confirm the structure. The band around 471 cm^{-1} is attributable to the mode of oxygen atom stretching [15]. The band at 788 cm^{-1} represents V–O–V asymmetric stretching modes while the 1004 cm^{-1} band corresponds to terminal oxygen stretching (V═O bond) [15,16] which confirms the formation of V_2O_5. The bands appeared at 1628 and 3436 cm^{-1} are due to the stretching vibrations in C═O and O—H, correspondingly [17]. Moreover, the carbon backbone stretching is associated with the peaks emerged at 2366 and 1094 cm^{-1}, respectively.

The broad and intense peaks in XPS studies (Fig. 1b) at 523.9 and 517.0 eV binding energies are assigned to V $2p_{1/2}$ and V $2p_{3/2}$, respectively for V 2p of V^{5+}, with a splitting of 6.9 eV [18]. A less intensed peak at 515.5 eV corresponds to minute V^{4+} content in V_2O_5/MWCNTs

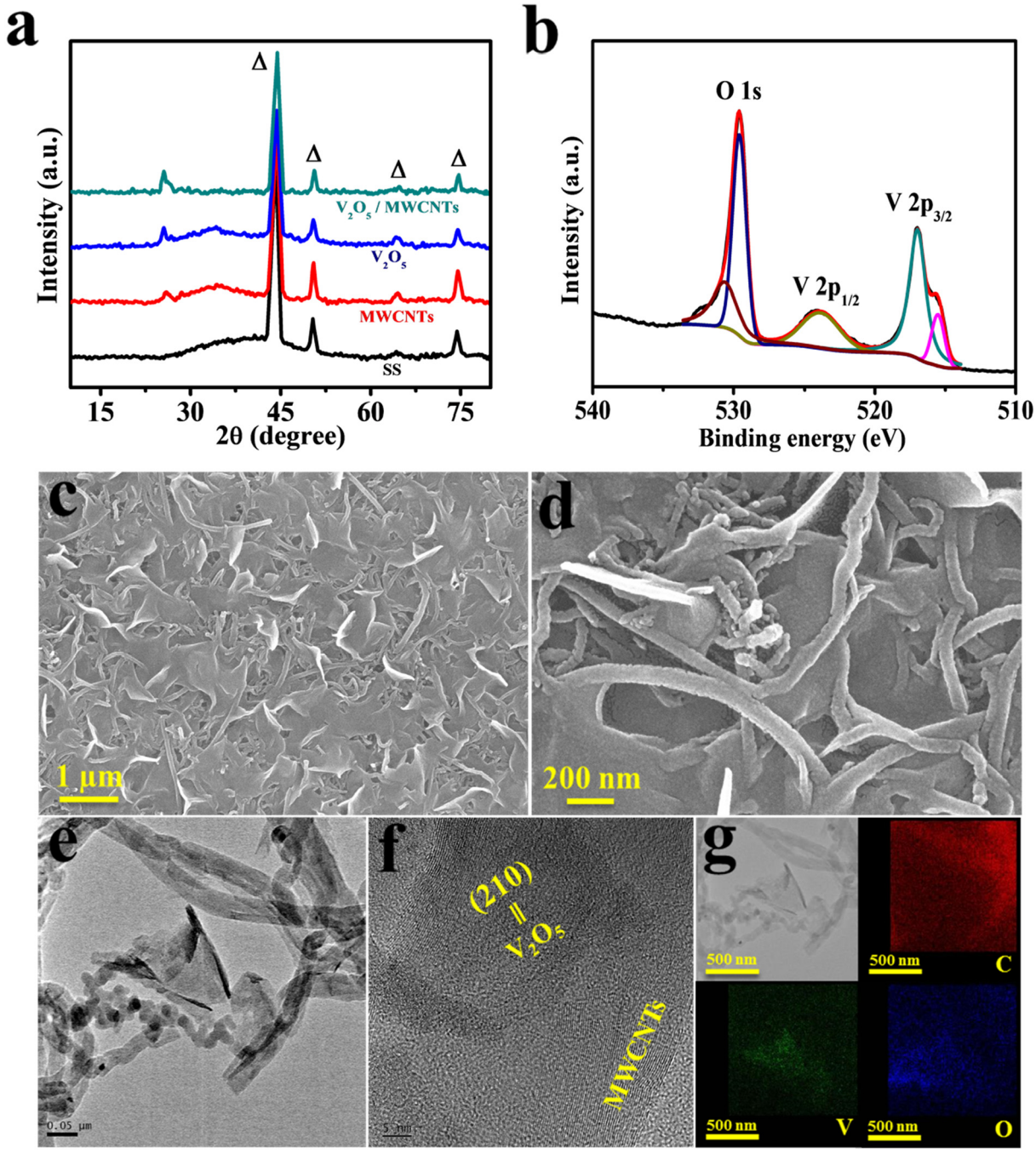

Fig. 1. (a) XRD patterns of MWCNTs, V_2O_5, and V_2O_5/MWCNTs thin films on SS substrates, (b) XPS core spectrum of V_2O_5/MWCNTs sample, (c, d) FESEM images of V_2O_5/MWCNTs thin film, (e, f) HRTEM images of V_2O_5/MWCNTs, (g) EDS elemental mapping of V_2O_5/MWCNTs.

composite [19]. The peak at 529.6 eV is allocated to the O 1s whereas a small inclusive peak at 530.6 eV is due to surface OH groups [20].

3.2. Morphological analysis

For supercapacitor point of view, morphology of the electroactive material significantly plays an influential role [21]. The FESEM images of composite film as shown in Fig. 1c, d exhibit a unique intermixed porous flakes surface morphology on MWCNTs surface. HRTEM analysis was also performed for the confirmation of definite size of nanoparticles along with the growth and distribution of crystallites. Fig. 1e displays the HRTEM image of as-synthesized V_2O_5 nanoflakes anchored MWCNTs. The fringes with lattice spacing of 0.34 nm revealed clearly in Fig. 1f associates with (210) planes indicating orthorhombic phase of V_2O_5, which is well supported by XRD studies. The EDS elemental mapping (Fig. 1g) demonstrates the distribution profile of vanadium, oxygen and carbon, confirming a homogeneous distribution of V_2O_5 flakes on MWCNTs surface.

3.3. Electrochemical performance of SSC device

Cyclic voltammetric (CV) curves at various scan rates of V_2O_5/MWCNTs electrode show high current response with a stable potential frame of 1 V in 2 M $LiClO_4$ electrolyte (Supplementary information S3). So, the CV plot performed at scan rate 100 mV/s of SSC device obviously shows an extended 2 V voltage window as depicted in Fig. 2a. With the

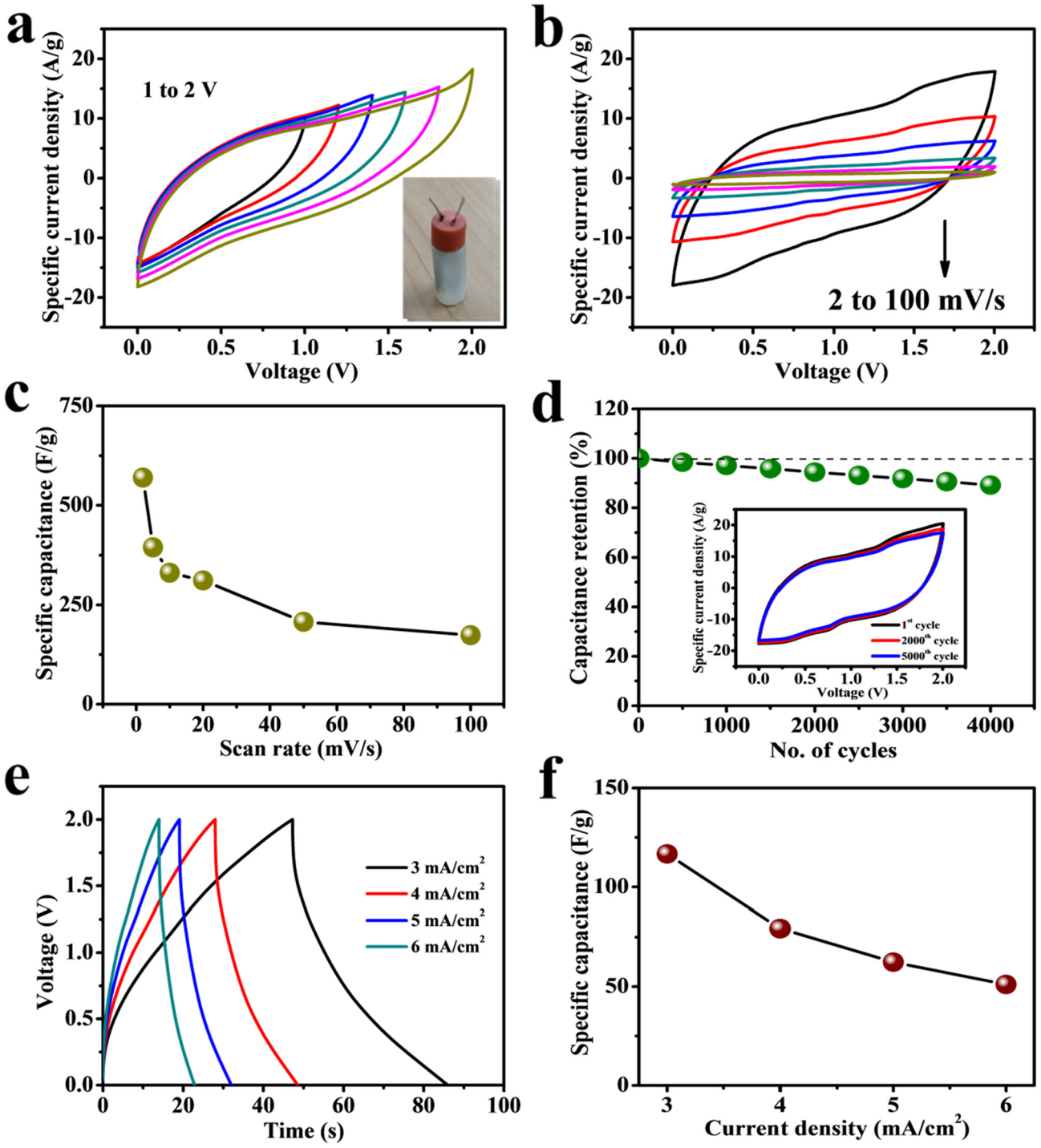

Fig. 2. Supercapacitive performance of SSC device in 2 M $LiClO_4$ electrolyte. (a) CV curves at scan rate of 100 mV/s for different voltage windows (1 to 2 V), (b) CV curves studied at various scan rates, (c) specific capacitances at different scan rates, (d) cycling stability for 4000 cycles at 100 mV/s scan rate, inset shows CV curves for various cycle numbers, (e) CD curves at different current densities ranging from 3 to 6 mA/cm^2, (f) specific capacitances at different current densities.

increment in scan rate from 2 to 100 mV/s (Fig. 2b), an improvement in current density was observed, but the shape of CV curves did not show apparent change which indicates exceptional supercapacitive characteristics of electrode material [22]. The specific capacitance value 569.7 F/g at scan rate of 2 mV/s (Fig. 2c) is attributed to active involvement in faradic redox reaction associated with pseudocapacitive mechanism [23]. Moreover, the volumetric capacitance involved in the cell is 592.5 F/cm^3 at scan rate of 2 mV/s. This value is comparable to the volumetric capacitance values of recently reported literatures [24–26]. The electrochemical inclusion of Li^+ ions inside V_2O_5 nanostructure can be defined by following reversible reaction based on redox mechanism [27].

$$xLi^+ + xe^- + V_2O_5 = Li_xV_2O_5 \quad (4)$$

The cycling life of device (Fig. 2d) was carried out for 4000 cycles at scan rate of 100 mV/s by analysing the CV plots. The device exhibits excellent capacitance retention of 89% with sustaining the shape of CV shapes even after 4000 cycles.

To examine the device performance, Galvanostatic charge/discharge (CD) test was carried out at various current densities and results are shown in Fig. 2e. At higher current densities, the fast diminishing of capacitance is due to internal resistances (IR drop) [28,29]. The GCD measurements yield outstanding capacitance of 111.7 F/g measured at a high current density of 3 mA/cm^2 (Fig. 2f), further validating observations obtained from the CV measurements. The V_2O_5 nanoflakes architecture on MWCNTs provides enormous electroactive sites, as a result electrolyte ions may simply penetrate to inner V_2O_5 layers with the maximum utilization of the electrode materials [30,31]. Energy and power densities were calculated using the discharge curves and represented in Ragone plot (Fig. 3a). The maximum energy density of 62 Wh/kg with great power density of 11.5 kW/kg shows quite encouraging framework for developing V_2O_5/MWCNTs as excellent electroactive material for electrochemical supercapacitors. The energy density of reported cell is significantly higher than previously reported symmetric devices with electrode materials such as porous carbon (7.22 Wh/kg) [32], MWCNTs (3.5 Wh/kg) [33], $MoSe_2$ (36.2 Wh/kg) [34], PEDOT:PSS/MWCNT (13.2 Wh/kg) [35], $ZnCo_2O_4$/rGO (11.44 Wh/kg) [36], ZnS/CNTs (22.3 Wh/kg) [37], Pt/n-CNT@PANI (30.22 Wh/kg) [38], waste paper fibers-RGO–MnO_2 (19.6 Wh/kg) [39], and N-doped cotton-derived carbon frameworks (NCCF)-rGO (20 Wh/kg) [40]. Even, energy density of the symmetric device is comparable with recent reports on high-performance asymmetric supercapacitor devices such as CoS//AC (5.3 Wh/kg) [41], CuS/3D graphene//3D graphene (5 Wh/kg) [42], $NiCo_2S_4$/polyaniline//AC (54.06 Wh/kg) [43], $NiCo_2O_4$/CC//porous graphene papers (PGP) (60.9 Wh/kg) [44], $NiCo_2O_4$@PPy//activated carbon (AC) (58.8 Wh/kg) [45], γ-MnS//eggplant derived AC (EDAC) (37.6 Wh/kg) [46], $CoMoO_4$@$NiMoO_4 \cdot xH_2O$//Fe_2O_3 (41.8 Wh/kg) [47], NiCo-LDH//carbon nanorods (59.2 Wh/kg) [48], MnO_2@PANI//3D graphene foam (GF) (37 Wh/kg) [49], and $Ni(OH)_2$/RGO/Ni//RGO aerogel/Ni (24.5 Wh/kg) [50]. All the evaluated electrochemical parameters are comparable with the reports on aqueous electrolyte based symmetric supercapacitor devices (Supplementary information S4).

To study the resistive factors of SSC device, electrochemical impedance spectroscopy (EIS) was analyzed (Fig. 3b). The solution resistance (R_S) signifying the ionic resistance of electrolyte is estimated by the non-zero intercept in real axis (Z′) from Nyquist plot [51]. The charge transfer resistance (R_{CT}) at electrolyte–electrode boundary is specified by semi-circular arc at high frequency region [52–55]. The SSC device showed very low R_S and R_{CT} values of 2.1 and 3.9 Ω/cm^2, respectively. In accordance with equivalent circuit, Nyquist plots were analyzed, which is illustrated in the inset of Fig. 3b. C_L and R_L are the leakage capacitance and resistance, respectively [56]. C_{DL} is related to double layer capacitance associated with MWCNTs while Warburg component (W) is responsible for shift between low and high frequency section [57–59]. The Bode plot shown in Fig. 3c exhibits the phase angle of −54°, displaying the capacitive behavior [60–62]. The device can intensely glow a red LED for 10 s after being charged with 2 V as shown in Fig. 3d–e, clearly demonstrating the commercial application of supercapacitor device (Supplementary video).

4. Conclusions

Liquid configured symmetric supercapacitor (SSC) device has been successfully configured by using simple and industry scalable chemical bath deposition (CBD) method to anchor V_2O_5 on to 'dip and dry' coated MWCNTs with $LiClO_4$ electrolyte as conducting mediator. The unique nanostructured morphology of V_2O_5/MWCNTs widens the electrochemical potential window up to 2.0 V which favors greater electrochemical features for excellent energy storage application. The SSC device exhibits

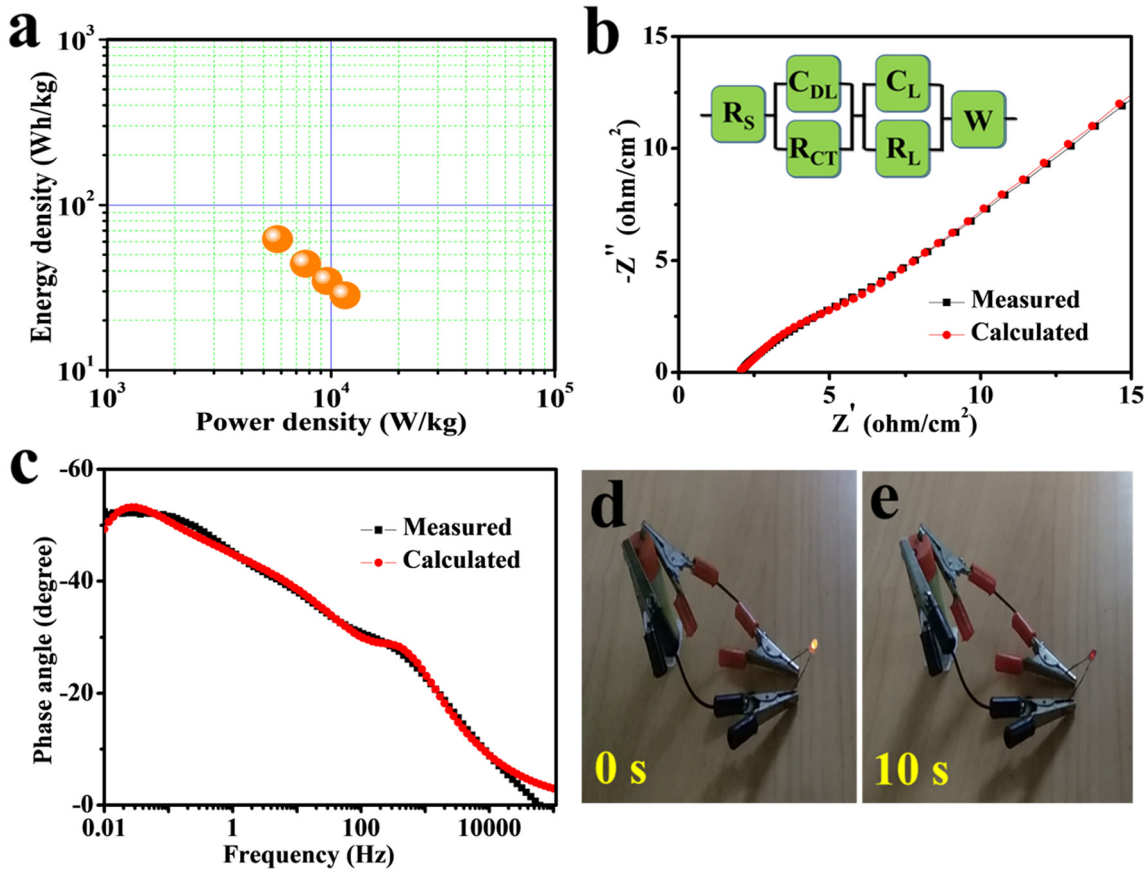

Fig. 3. (a) Ragone plot, (b) Nyquist plot in the frequency ranging from 100 mHz to 100 kHz, inset displays the related equivalent circuit, (c) Bode plot, (d, e) demonstration of SSC device discharging through red LED for 10 s.

an improved specific capacitance of 569.7 F/g and advanced energy density of 62 Wh/kg including long-term cyclic stability. The effective effort to light a commercial LED displays that SSC cell has good prospect to be directed in energy and convenient electronics applications.

Supplementary data to this article can be found online at https://doi.org/10.1016/j.matdes.2019.107972.

CRediT authorship contribution statement

Shilpa A. Pande: Conceptualization, Data curation, Formal analysis, Funding acquisition, Investigation, Methodology, Project administration, Resources, Software, Supervision, Validation, Visualization, Writing - original draft, Writing - review & editing. **Bidhan Pandit:** Conceptualization, Data curation, Formal analysis, Investigation, Methodology, Resources, Software, Supervision, Validation, Visualization, Writing - review & editing. **Babasaheb R. Sankapal:** Conceptualization, Project administration, Resources, Supervision, Validation, Visualization, Writing - review & editing.

Acknowledgements

S.A. gratefully acknowledges the support from Nano Materials and Device Laboratory, Visvesvaraya National Institute of Technology.

Data availability

The raw/processed data required to reproduce these findings cannot be shared at this time as the data also forms part of an ongoing study.

References

[1] P. Simon, Y. Gogotsi, Materials for electrochemical capacitors, Nat. Mater. 7 (2008) 845.
[2] M. Ghosh, V. Vijayakumar, R. Soni, S. Kurungot, A rationally designed self-standing V_2O_5 electrode for high voltage non-aqueous all-solid-state symmetric (2.0 V) and asymmetric (2.8 V) supercapacitors, Nanoscale 10 (2018) 8741–8751.
[3] J. Kim, J.H. Kim, K. Ariga, Redox-active polymers for energy storage Nanoarchitectonics, Joule 1 (2017) 739–768.
[4] R. Córdoba, A. Kuhn, J.C. Pérez-Flores, E. Morán, J.M. Gallardo-Amores, F. García-Alvarado, Sodium insertion in high pressure β-V_2O_5: a new high capacity cathode material for sodium ion batteries, J. Power Sources 422 (2019) 42–48.
[5] Y. Zhang, W. Li, M. Fan, F. Zhang, J. Zhang, X. Liu, H. Zhang, C. Huang, H. Li, Preparation of W- and Mo-doped VO_2(M) by ethanol reduction of peroxovanadium complexes and their phase transition and optical switching properties, J. Alloys Compd. 544 (2012) 30–36.
[6] S.A. Han, J. Lee, K. Shim, J. Lin, M. Shahabuddin, J.-W. Lee, S.-W. Kim, M.-S. Park, J.H. Kim, Strategically designed zeolitic imidazolate frameworks for controlling the degree of graphitization, Bull. Chem. Soc. Jpn. 91 (2018) 1474–1480.
[7] J. Kim, C. Young, J. Lee, Y.-U. Heo, M.-S. Park, M.S.A. Hossain, Y. Yamauchi, J.H. Kim, Nanoarchitecture of MOF-derived nanoporous functional composites for hybrid supercapacitors, J. Mater. Chem. A 5 (2017) 15065–15072.
[8] J. Kim, C. Young, J. Lee, M.-S. Park, M. Shahabuddin, Y. Yamauchi, J.H. Kim, CNTs grown on nanoporous carbon from zeolitic imidazolate frameworks for supercapacitors, Chem. Commun. 52 (2016) 13016–13019.
[9] Y. Wu, G. Gao, H. Yang, W. Bi, X. Liang, Y. Zhang, G. Zhang, G. Wu, Controlled synthesis of V_2O_5/MWCNT core/shell hybrid aerogels through a mixed growth and self-assembly methodology for supercapacitors with high capacitance and ultralong cycle life, J. Mater. Chem. A 3 (2015) 15692–15699.
[10] M. Lee, S.K. Balasingam, H.Y. Jeong, W.G. Hong, H.-B.-R. Lee, B.H. Kim, Y. Jun, One-step hydrothermal synthesis of graphene decorated V_2O_5 nanobelts for enhanced electrochemical energy storage, Sci. Rep. 5 (2015) 8151.
[11] B.-H. Kim, C.H. Kim, K.S. Yang, A. Rahy, D.J. Yang, Electrospun vanadium pentoxide/carbon nanofiber composites for supercapacitor electrodes, Electrochim. Acta 83 (2012) 335–340.
[12] B. Pandit, D.P. Dubal, B.R. Sankapal, Large scale flexible solid state symmetric supercapacitor through inexpensive solution processed V_2O_5 complex surface architecture, Electrochim. Acta 242 (2017) 382–389.
[13] K. Takahashi, S.J. Limmer, Y. Wang, G. Cao, Synthesis and electrochemical properties of single-crystal V_2O_5 nanorod arrays by template-based electrodeposition, J. Phys. Chem. B 108 (2004) 9795–9800.
[14] B. Pandit, B.R. Sankapal, P.M. Koinkar, Novel chemical route for CeO_2/MWCNTs composite towards highly bendable solid-state supercapacitor device, Sci. Rep. 9 (2019) 5892.
[15] J. Chu, Z. Kong, D. Lu, W. Zhang, X. Wang, Y. Yu, S. Li, X. Wang, S. Xiong, J. Ma, Hydrothermal synthesis of vanadium oxide nanorods and their electrochromic performance, Mater. Lett. 166 (2016) 179–182.
[16] W. Kang, C. Yan, X. Wang, C.Y. Foo, A.W. Ming Tan, K.J. Zhi Chee, P.S. Lee, Green synthesis of nanobelt-membrane hybrid structured vanadium oxide with high electrochromic contrast, J. Mater. Chem. C 2 (2014) 4727–4732.
[17] B. Pandit, L.K. Bommineedi, B.R. Sankapal, Electrochemical engineering approach of high performance solid-state flexible supercapacitor device based on chemically synthesized VS_2 nanoregime structure, J. Energy Chem. 31 (2019) 79–88.
[18] J. Qin, M. Zhang, S. Rajendran, X. Zhang, R. Liu, Facile synthesis of graphene-$AgVO_3$ nanocomposite with excellent supercapacitor performance, Mater. Chem. Phys. 212 (2018) 30–34.
[19] K.-H. Chang, C.-C. Hu, $H_2V_3O_8$ single-crystal nanobelts: hydrothermal preparation and formation mechanism, Acta Mater. 55 (2007) 6192–6197.
[20] C.-C. Hu, C.-M. Huang, K.-H. Chang, Anodic deposition of porous vanadium oxide network with high power characteristics for pseudocapacitors, J. Power Sources 185 (2008) 1594–1597.
[21] B. Pandit, V.S. Devika, B.R. Sankapal, Electroless-deposited Ag nanoparticles for highly stable energy-efficient electrochemical supercapacitor, J. Alloys Compd. 726 (2017) 1295–1303.
[22] B. Pandit, B.R. Sankapal, Highly conductive energy efficient electroless anchored silver nanoparticles on MWCNTs as a supercapacitive electrode, New J. Chem. 41 (2017) 10808–10814.
[23] S.A. Pande, B. Pandit, B.R. Sankapal, Facile chemical route for multiwalled carbon nanotube/mercury sulfide nanocomposite: high performance supercapacitive electrode, J. Colloid Interface Sci. 514 (2018) 740–749.
[24] C. Zhang, B. Anasori, A. Seral-Ascaso, S.-H. Park, N. McEvoy, A. Shmeliov, G.S. Duesberg, J.N. Coleman, Y. Gogotsi, V. Nicolosi, Transparent, flexible, and conductive 2D titanium carbide (MXene) films with high volumetric capacitance, Adv. Mater. 29 (2017) 1702678.
[25] M. Ghidiu, M.R. Lukatskaya, M.-Q. Zhao, Y. Gogotsi, M.W. Barsoum, Conductive two-dimensional titanium carbide 'clay' with high volumetric capacitance, Nature 516 (2014) 78.
[26] Z.-S. Wu, K. Parvez, A. Winter, H. Vieker, X. Liu, S. Han, A. Turchanin, X. Feng, K. Müllen, Layer-by-layer assembled heteroatom-doped graphene films with ultrahigh volumetric capacitance and rate capability for micro-supercapacitors, Adv. Mater. 26 (2014) 4552–4558.
[27] J. Wu, D. Qiu, H. Zhang, H. Cao, W. Wang, Z. Liu, T. Tian, L. Liang, J. Gao, F. Zhuge, Flexible electrochromic V_2O_5 thin films with ultrahigh coloration efficiency on graphene electrodes, J. Electrochem. Soc. 165 (2018) D183–D189.
[28] B. Pandit, N. Kumar, P.M. Koinkar, B.R. Sankapal, Solution processed nanostructured cerium oxide electrode: electrochemical engineering towards solid-state symmetric supercapacitor device, J. Electroanal. Chem. 839 (2019) 96–107.
[29] B. Pandit, S.R. Dhakate, B.P. Singh, B.R. Sankapal, Free-standing flexible MWCNTs bucky paper: extremely stable and energy efficient supercapacitive electrode, Electrochim. Acta 249 (2017) 395–403.
[30] J. Zhao, Y. Li, G. Wang, T. Wei, Z. Liu, K. Cheng, K. Ye, K. Zhu, D. Cao, Z. Fan, Enabling high-volumetric-energy-density supercapacitors: designing open, low-tortuosity heteroatom-doped porous carbon-tube bundle electrodes, J. Mater. Chem. A 5 (2017) 23085–23093.
[31] J. Zhao, G. Wang, R. Hu, K. Zhu, K. Cheng, K. Ye, D. Cao, Z. Fan, Ultrasmall-sized SnS nanosheets vertically aligned on carbon microtubes for sodium-ion capacitors with high energy density, J. Mater. Chem. A 7 (2019) 4047–4054.
[32] X. Li, K. Liu, Z. Liu, Z. Wang, B. Li, D. Zhang, Hierarchical porous carbon from hazardous waste oily sludge for all-solid-state flexible supercapacitor, Electrochim. Acta 240 (2017) 43–52.
[33] S. Li, C. Xuebo, L. Lei, W. Qiaodi, Y. Huating, G. Li, M. Changjie, S. Jiming, Z. Shengyi, N. Helin, General method for large-area films of carbon nanomaterials and application of a self-assembled carbon nanotube film as a high-performance electrode material for an all-solid-state supercapacitor, Adv. Funct. Mater. 27 (2017), 1700474.
[34] Y. Qiu, X. Li, M. Bai, H. Wang, D. Xue, W. Wang, J. Cheng, Flexible full-solid-state supercapacitors based on self-assembly of mesoporous $MoSe_2$ nanomaterials, Inorg. Chem. Front. 4 (2017) 675–682.
[35] D. Zhao, Q. Zhang, W. Chen, X. Yi, S. Liu, Q. Wang, Y. Liu, J. Li, X. Li, H. Yu, Highly flexible and conductive cellulose-mediated PEDOT:PSS/MWCNT composite films for supercapacitor electrodes, ACS Appl. Mater. Interfaces 9 (2017) 13213–13222.
[36] M.I. Kyu, Y. Seonno, O. Jungwoo, Three-dimensional hierarchically mesoporous $ZnCo_2O_4$ nanowires grown on graphene/sponge foam for high-performance, flexible, all-solid-state supercapacitors, Chem. Eur. J. 23 (2017) 597–604.
[37] X. Hou, T. Peng, J. Cheng, Q. Yu, R. Luo, Y. Lu, X. Liu, J.-K. Kim, J. He, Y. Luo, Ultrathin ZnS nanosheet/carbon nanotube hybrid electrode for high-performance flexible all-solid-state supercapacitor, Nano Res. 10 (2017) 2570–2583.
[38] Y. Wu, Q. Wang, T. Li, D. Zhang, M. Miao, Fiber-shaped supercapacitor and electrocatalyst containing of multiple carbon nanotube yarns and one platinum wire, Electrochim. Acta 245 (2017) 69–78.
[39] H. Su, P. Zhu, L. Zhang, F. Zhou, G. Li, T. Li, Q. Wang, R. Sun, C. Wong, Waste to wealth: a sustainable and flexible supercapacitor based on office waste paper electrodes, J. Electroanal. Chem. 786 (2017) 28–34.
[40] Y.-M. Fan, W.-L. Song, X. Li, L.-Z. Fan, Assembly of graphene aerogels into the 3D biomass-derived carbon frameworks on conductive substrates for flexible supercapacitors, Carbon 111 (2017) 658–666.
[41] K. Subramani, N. Sudhan, R. Divya, M. Sathish, All-solid-state asymmetric supercapacitors based on cobalt hexacyanoferrate-derived CoS and activated carbon, RSC Adv. 7 (2017) 6648–6659.
[42] Z. Tian, H. Dou, B. Zhang, W. Fan, X. Wang, Three-dimensional graphene combined with hierarchical CuS for the design of flexible solid-state supercapacitors, Electrochim. Acta 237 (2017) 109–118.

[43] X. He, Q. Liu, J. Liu, R. Li, H. Zhang, R. Chen, J. Wang, High-performance all-solid-state asymmetrical supercapacitors based on petal-like $NiCo_2S_4$/polyaniline nanosheets, Chem. Eng. J. 325 (2017) 134–143.
[44] Z. Gao, W. Yang, J. Wang, N. Song, X. Li, Flexible all-solid-state hierarchical $NiCo_2O_4$/porous graphene paper asymmetric supercapacitors with an exceptional combination of electrochemical properties, Nano Energy 13 (2015) 306–317.
[45] D. Kong, W. Ren, C. Cheng, Y. Wang, Z. Huang, H.Y. Yang, Three-dimensional $NiCo_2O_4$@polypyrrole coaxial nanowire arrays on carbon textiles for high-performance flexible asymmetric solid-state supercapacitor, ACS Appl. Mater. Interfaces 7 (2015) 21334–21346.
[46] T. Chen, Y. Tang, Y. Qiao, Z. Liu, W. Guo, J. Song, S. Mu, S. Yu, Y. Zhao, F. Gao, All-solid-state high performance asymmetric supercapacitors based on novel MnS nanocrystal and activated carbon materials, Sci. Rep. 6 (2016), 23289.
[47] J. Wang, L. Zhang, X. Liu, X. Zhang, Y. Tian, X. Liu, J. Zhao, Y. Li, Assembly of flexible $CoMoO_4$@$NiMoO_4 \cdot xH_2O$ and Fe_2O_3 electrodes for solid-state asymmetric supercapacitors, Sci. Rep. 7 (2017), 41088.
[48] T. Wang, S. Zhang, X. Yan, M. Lyu, L. Wang, J. Bell, H. Wang, 2-Methylimidazole-derived Ni–co layered double hydroxide Nanosheets as high rate capability and high energy density storage material in hybrid supercapacitors, ACS Appl. Mater. Interfaces 9 (2017) 15510–15524.
[49] K. Ghosh, C.Y. Yue, M.M. Sk, R.K. Jena, Development of 3D urchin-shaped coaxial manganese dioxide@polyaniline (MnO_2@PANI) composite and self-assembled 3D pillared graphene foam for asymmetric all-solid-state flexible supercapacitor application, ACS Appl. Mater. Interfaces 9 (2017) 15350–15363.
[50] K. Lu, J. Zhang, Y. Wang, J. Ma, B. Song, H. Ma, Interfacial deposition of three-dimensional nickel hydroxide nanosheet-graphene aerogel on Ni wire for flexible fiber asymmetric supercapacitors, ACS Sustain. Chem. Eng. 5 (2017) 821–827.
[51] D. Wang, L. Xu, J. Nai, T. Sun, A versatile co-activation strategy towards porous carbon nanosheets for high performance ionic liquid based supercapacitor applications, J. Alloys Compd. 786 (2019) 109–117.
[52] B. Pandit, D.P. Dubal, P. Gómez-Romero, B.B. Kale, B.R. Sankapal, V_2O_5 encapsulated MWCNTs in 2D surface architecture: complete solid-state bendable highly stabilized energy efficient supercapacitor device, Sci. Rep. 7 (2017), 43430.
[53] S.A. Pande, B. Pandit, B.R. Sankapal, Electrochemical approach of chemically synthesized HgS nanoparticles as supercapacitor electrode, Mater. Lett. 209 (2017) 97–101.
[54] Y. Jia, Y. Lin, Y. Ma, W. Shi, Hierarchical MnS_2-MoS_2 nanotubes with efficient electrochemical performance for energy storage, Mater. Des. 160 (2018) 1071–1079.
[55] E. Brown, P. Yan, H. Tekik, A. Elangovan, J. Wang, D. Lin, J. Li, 3D printing of hybrid MoS_2-graphene aerogels as highly porous electrode materials for sodium ion battery anodes, Mater. Des. 170 (2019), 107689.
[56] M. Liu, M. Xia, R. Qi, Q. Ma, M. Zhao, Z. Zhang, X. Lu, Lyotropic liquid crystal as an electrolyte additive for suppressing self-discharge of supercapacitors, ChemElectroChem 6 (2019) 2531–2535.
[57] B. Pandit, G.K. Sharma, B.R. Sankapal, Chemically deposited Bi_2S_3:PbS solid solution thin film as supercapacitive electrode, J. Colloid Interface Sci. 505 (2017) 1011–1017.
[58] W.K. Jung, C. Baek, J.-H. Kim, S. Moon, D.S. Kim, Y.H. Jung, D.K. Kim, A highly-aligned lamellar structure of ice-templated $LiFePO_4$ cathode for enhanced rate capability, Mater. Des. 139 (2018) 89–95.
[59] X. Zhang, X. Huang, X. Zhang, L. Xia, B. Zhong, T. Zhang, G. Wen, Cotton/rGO/carbon-coated SnO_2 nanoparticle-composites as superior anode for lithium ion battery, Mater. Des. 114 (2017) 234–242.
[60] B. Pandit, S.S. Karade, B.R. Sankapal, Hexagonal VS_2 anchored MWCNTs: first approach to design flexible solid-state symmetric supercapacitor device, ACS Appl. Mater. Interfaces 9 (2017) 44880–44891.
[61] S. Sankar, A.T.A. Ahmed, A.I. Inamdar, H. Im, Y.B. Im, Y. Lee, D.Y. Kim, S. Lee, Biomass-derived ultrathin mesoporous graphitic carbon nanoflakes as stable electrode material for high-performance supercapacitors, Mater. Des. 169 (2019), 107688.
[62] A.V. Radhamani, M. Krishna Surendra, M.S. Ramachandra Rao, Tailoring the supercapacitance of Mn_2O_3 nanofibers by nanocompositing with spinel-$ZnMn_2O_4$, Mater. Des. 139 (2018) 162–171.